High-pressure *hP*3 yttrium allotrope with $CaHg_2$-type structure as a prototype of the *hP*3 rare-earth hydride series

Alena Aslandukova,[1,*] Andrey Aslandukov,[1,2] Dominique Laniel,[3] Saiana Khandarkhaeva,[2] Gerd Steinle-Neumann,[1] Timofey Fedotenko,[4] Sergey V. Ovsyannikov,[1] Yuqing Yin,[2,5] Fariia Iasmin Akbar,[1] Konstantin Glazyrin,[4] Michael Hanfland,[6] Leonid Dubrovinsky,[1] and Natalia Dubrovinskaia[2,7]

[1]*Bavarian Research Institute of Experimental Geochemistry and Geophysics (BGI), University of Bayreuth, Universitaetsstrasse 30, 95440 Bayreuth, Germany*

[2]*Material Physics and Technology at Extreme Conditions, Laboratory of Crystallography, University of Bayreuth, 95440 Bayreuth, Germany*

[3]*Centre for Science at Extreme Conditions and School of Physics and Astronomy, University of Edinburgh, Edinburgh EH93FD, United Kingdom*

[4]*Deutsches Elektronen-Synchrotron DESY, Notkestr. 85, 22607 Hamburg, Germany*

[5]*State Key Laboratory of Crystal Materials, Shandong University, Jinan 250100, China*

[6]*European Synchrotron Radiation Facility (ESRF), BP 220, 38043 Grenoble Cedex, France*

[7]*Department of Physics, Chemistry and Biology (IFM), Linköping University, SE-581 83 Linköping, Sweden*

(Received 28 September 2022; revised 7 December 2022; accepted 9 December 2022; published 9 January 2023)

A high-pressure (HP) yttrium allotrope, *hP*3-Y (space group $P6/mmm$), was synthesized in a multi-anvil press at 20 GPa and 2000 K which is recoverable to ambient conditions. Its relative stability and electronic properties were investigated using density functional theory calculations. A *hP*3-Y derivative hydride, *hP*3-YHx, with a variable hydrogen content ($x = 2.8$, 3, 2.4), was synthesized in diamond anvil cells by the direct reaction of yttrium with paraffin oil, hydrogen gas, and ammonia borane upon laser heating to ∼3000 K at 51, 45 and 38 GPa, respectively. Room-temperature decompression leads to gradual reduction and eventually the complete loss of hydrogen at ambient conditions. Isostructural *hP*3-NdHx and *hP*3-GdHx hydrides were synthesized from Nd and Gd metals and paraffin oil, suggesting that the *hP*3-Y structure type may be common for rare-earth elements. Our results expand the list of allotropes of trivalent lanthanides and their hydrides and suggest that they should be considered in the context of studies of HP behavior and properties of this broad class of materials.

DOI: 10.1103/PhysRevB.107.014103

I. INTRODUCTION

The study of rare-earth (RE) metal hydrides is one of the most interesting research topics in current solid-state physics due to the search for high-T_C superconductivity, as key advances in experimental techniques lead to the synthesis of hydrides at high pressure (HP) that were then reported to become high-T_C superconductors [1]. Recent publications on record high-T_C superconductivity in LaH_{10} at 250–260 K [2,3] and HP–high-temperature (HT) synthesis of CeH_9 [4], UH_7, UH_8 [5], ThH_{10} [6], as well as a series of yttrium hydrides (YH_9, YH_6, YH_4) [7–9] motivated us to study the Y-H system at HP. The reason is that there are still many open questions regarding, for example, the origin of the superconducting effect and the structure (or chemical composition) of the materials for which the phenomenon is described [10–12]. Some problems with the currently available experimental data interpretation may be associated with the synthesis technique: hydrides at HP are often obtained by heating metals embedded in paraffin oil or ammonia borane [3,6–8,13–15], and one cannot exclude that other nonhydride phases (e.g., carbon and boron compounds) may form in the system under investigation [16,17], and their properties can influence the measurements of superconductivity.

Determining the crystal structure and composition of hydrides is a very complex task since usual experimental methods such as x-ray diffraction (XRD) are not capable of determining the positions of hydrogen atoms. Instead, the amount of hydrogen in a metal hydride synthesized at HP is often estimated by comparing its unit cell volume with that of the metal at the same pressure. This requires information about the equation of state (EoS) of the metal and an understanding of the volume changes with hydrogen content, the latter typically determined by using density functional theory (DFT) calculations.

The EoS of yttrium at pressures up to 180 GPa was published recently [18]. At ambient pressure, yttrium possesses a hexagonal close-packed (hcp) structure, *hP*2-Y in Pearson's notation (space group $P6_3/mmc$). Under compression up to 100 GPa at room temperature, yttrium undergoes a series of phase transitions typical for RE metals, with the structures differing only in the stacking of close-packed atomic layers: hcp ($P6_3/mmc$, *hP*2) → α-Sm type (R-3m, *hR*9) → double hcp (dhcp; $P6_3/mmc$, *hP*4) → face-centered cubic (fcc; Fm-3m, *cF*4) → distorted-*cF*4 (R-3m, *hR*24) [18]. The sequential

*alena.aslandukova@uni-bayreuth.de

structural transitions are well understood with the *s-d* electronic transition model [19–21]. It should be noted that this sequence of transitions has been reported based on powder XRD data upon the compression of yttrium in the absence of a pressure-transmitting medium. Interpretation of powder diffraction data is not trivial, considering the coexistence of several phases due to the sluggish character of transformations at room temperature and similarities of the *hP*2, *hR*9, *hP*4, and *cF*4 structures, which results in a significant overlap of diffraction peaks of different phases. Research on the behavior of yttrium at HP-HT conditions is lacking.

While at pressures >150 GPa the synthesis of a number of yttrium hydrides YH_4 YH_6, YH_7, and YH_9 [7,8] was reported, at lower pressures (up to 90 GPa), only hcp YH_3 and fcc YH_x ($x = 2$–3) are known [22–24]. It was suggested that yttrium hydride YH_x has a continuous hcp-to-fcc structure phase transition at pressures from 12.5 to 22 GPa with an intermediate yet uncharacterized structure state in between [24]. Notably, all reported high-T_C yttrium hydrides were synthesized by heating of Y in H_2 gas or in ammonia borane at pressures $>\sim$ 90 GPa; at lower pressures, HT experiments in the Y-H system have not been carried out.

Here, we report on the synthesis and characterization of a HP yttrium allotrope, *hP*3-Y, formed upon heating of Y to ∼2000 K at 20 GPa in a multi-anvil (MA) apparatus. Derivative hydrides, *hP*3-YH_x, were obtained from Y and various hydrogen precursors in diamond anvil cells (DACs) laser heated to ∼3000 K at 38, 45, and 51 GPa. On decompression to 14 GPa, these hydrides were observed to gradually lose hydrogen. We have extended our study by synthesizing Nd and Gd hydrides isostructural to *hP*3-YH_x, allowing us to generalize our conclusions.

II. EXPERIMENTAL METHODS

A. Sample preparation

1. MA synthesis

Samples of the *hP*3 yttrium allotrope were synthesized at HP-HT conditions using the multiton MA presses at the BGI (Bayreuth, Germany) [25] at a pressure of 20 GPa and a temperature of 2000 K; synthesis times were 24 h. We used a standard MA assembly that included a graphite cylindrical sample capsule, a $LaCrO_3$ heater, an octahedral container, and other parts [25]. Using single-crystal XRD (SCXRD), we selected high-quality crystals from the recovered samples and used them for further investigations.

2. Synthesis in DAC

The BX90-type large x-ray aperture DAC equipped with Boehler-Almax-type diamonds (culet diameter is 250 mm) was used for SCXRD studies [26,27]. Rhenium foil preindented to a thickness of ∼20 μm and a hole of ∼100 μm in diameter drilled in the center of the indentation served as a sample chamber. A piece of yttrium (or Nd/Gd) was placed in the sample chamber filled with paraffin oil (DAC1, DAC4, and DAC5) or ammonia borane (DAC2). The sample chamber of DAC3 was loaded with hydrogen gas using the HP gas loading system at Petra III (DESY, Hamburg, Germany). The pressure was determined using the EoS of Re [28,29] (for all DACs except DAC3) and additionally monitored by the Raman signal from the diamond anvils [30]. Samples were compressed up to 51 GPa (DAC1), 38 GPa (DAC2), 42 GPa (DAC3), 40 GPa (DAC4), and 45 GPa (DAC5) and laser heated to ∼3000(200) K. Laser heating of the samples was performed using an in-house setup [31] equipped with two YAG lasers (1064 nm central wavelength).

B. XRD measurements and data analysis procedure

XRD measurements for DAC1, DAC2, and DAC3 were performed at beamline P02.2 of Petra III (DESY, Hamburg, Germany) with the x-ray beam ($\lambda = 0.2891$ Å) focused down to $1.8\times2\,\mu m^2$ by a Kirkpatrick-Baez mirror system, and diffraction patterns were collected on a PerkinElmer 1621 XRD flat-panel detector. XRD measurements for DAC3, DAC4, and samples from MA1 and MA2 were performed at the ID15B beamline (ESRF, Grenoble, France) with an x-ray beam ($\lambda = 0.4103$ Å) focused to a size of $8\times8\,\mu m^2$, and the XRD patterns were collected on an Eiger2X CdTe 9M hybrid photon-counting pixel detector. For SCXRD measurements, samples were rotated around a vertical ω axis in a range of ±35°. The XRD images were collected with an angular step $\Delta\omega = 0.5°$. The CRYSALISPRO software package [32] was used for the analysis of the SCXRD data (indexing, data integration, frame scaling, and absorption correction). A single crystal of $(Mg_{1.93}, Fe_{0.06})(Si_{1.93}, Al_{0.06})O_6$ orthoenstatite [*Pbca*, $a = 18.2391(3)$, $b = 8.8117(2)$, and $c = 5.18320(10)$ Å] was used to calibrate the instrument model of the CRYSALISPRO software. The DAFI program [33] was used for the search of reflection groups belonging to the individual single-crystal domains. Using the OLEX2 software package [34], the structures were solved with the SHELXT structure solution program [35] using intrinsic phasing and refined with the SHELXL [36] refinement package using least-squares minimization. Crystal structure visualizations were made with VESTA software [37]. The experimental EoSs of the synthesized materials were obtained by fitting the pressure-volume data using the EoSFit7-GUI [38].

III. COMPUTATIONAL DETAILS

The properties of the systems were determined via first-principles calculations using Kohn-Sham DFT with the generalized gradient approximation by Perdew-Burke-Ernzerhof [39] for the exchange-correlation energy implemented within the projector augmented-wave method [40] for describing the interaction between the core and the valence electrons (4*s*4*p*5*s*4*d*) in the Vienna *Ab initio* Simulation Package (VASP) [41]. We used the Monkhorst-Pack scheme with $8\times8\times14$ *k*-points for Brillouin zone sampling and an energy cutoff for the plane-wave expansion of 600 eV, with which total energies are converged to better than 2 meV/atom. EoS and static enthalpy calculations were performed via variable-cell structural relaxations for 11 volumes that cover the pressure range of 0–50 GPa. The phonon calculations were performed in the harmonic approximation with the help of PHONOPY software using density functional perturbation theory for a $2\times2\times2$ supercell with respectively adjusted *k*-points [42]. In our calculations, temperature, configurational entropy, and the

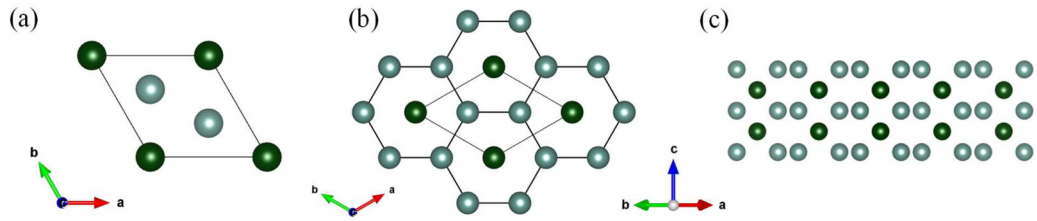

FIG. 1. Crystal structure of the *hP*3 yttrium allotrope. (a) Unit cell, (b) graphenelike nets of Y2 atoms alternating with nets of Y1 atoms along the *c* direction, and (c) a view along the [110] direction showing the stacking of nets of yttrium atoms (oriented perpendicular to the page) along the *c* direction. Yttrium atoms, Y1 and Y2, are shown in dark green and light green, respectively.

entropy contribution due to lattice vibrations were neglected. Fermi surface visualization was made with XCRYSDEN software [43].

IV. RESULTS AND DISCUSSION

The *hP*3 yttrium allotrope was synthesized in HP-HT experiments in a MA press (Table S1 in the Supplemental Material [44]): a piece of yttrium metal was compressed to 20 GPa and heated to 2000 K for 24 h (MA1 and MA2), with two independent MA experiments at the same conditions yielding the same result. The *hP*3 yttrium allotrope, along with two known carbides [45], cubic NaCl-type YC_x and Y_2C_3 (products of yttrium interaction with the graphite capsule, Table S1 in the Supplemental Material [44]), was characterized by in-house and synchrotron powder and SCXRD from products of both MA experiments. The details of the sample preparation, data collection, structure determination, and refinement are described in the Supplemental Material [44].

The yttrium allotrope has a hexagonal *hP*3 structure (space group $P6/mmm$, $Z = 3$) with unit cell parameters $a = 5.7809(10)$ Å, $c = 3.3453(5)$ Å, and $V = 96.82(4)$ Å^3 at 1 bar. Yttrium atoms occupy two crystallographically independent positions: Y1 at the 1*a* (0, 0, 0) site and Y2 at the 2*d* ($\frac{1}{3}$, $\frac{2}{3}$, $\frac{1}{2}$) site [Fig. 1(a)], like Ca and Hg atoms, respectively, in the $CaHg_2$ structure (58901-ICSD). The structure can be described as an alternation of graphenelike nets of Y2 atoms with nets of Y1 atoms along the *c* direction [Figs. 1(b)–1(c)]. All distances between Y1 and Y2 are equal to 3.7333(5) Å, which is significantly longer than the distances between Y1 and Y1 or Y2 and Y2, 3.3453(5) Å and 3.3376(6) Å, respectively. Interestingly, the Y1-Y1 and Y2-Y2 distances are shorter than the Y-Y distance in hcp yttrium, *hP*2-Y [$d_{Y-Y} = 3.5559(5)$ Å, data from 660002-ICSD]. Titanium also has an *hP*2 allotrope, α-Ti, and an *hP*3-Ti allotrope, ω-Ti (space group $P6/mmm$), both isostructural to *hP*2-Y and *hP*3-Y, respectively, with Ti2-Ti2 distances in *hP*3-Ti also shorter than Ti-Ti in *hP*2-Ti [46,47]. The densities of *hP*3-Y and *hP*2-Y (4.57 and 4.47 g/cm^3 at 1 bar, respectively) differ by ∼1.7%, similar to titanium (4.61 g/cm^3 for ω-Ti and 4.51 g/cm^3 for α-Ti at 1 bar, data from 52521- and 253841-ICSD, respectively).

To gain deeper insight into the stability and pressure-volume behavior of *hP*3-Y, we performed calculations on the full relaxation of the structural model of *hP*3-Y at 1 bar using DFT, which results in unit cell parameters and atomic coordinates that perfectly agree with the experimental data at ambient conditions (Table S2 in the Supplemental Material [44]). To assess the dynamical stability of *hP*3-Y, harmonic phonon dispersion calculations along the high-symmetry directions of the Brillouin zone were made, showing that hexagonal *hP*3-Y is dynamically stable at 1 bar [Fig. 2(a)]. Static enthalpy calculations up to 50 GPa reproduced the experimentally known sequence of yttrium phase transitions, hcp ($P6_3/mmc$, *hP*2) → α-Sm type (R-3m, *hR*9) → dhcp ($P6_3/mmc$, *hP*4), but with a little shift of transition pressure values. Over the whole pressure range considered, the *hP*3-Y allotrope is thermodynamically unfavorable [Fig. 2(b)]. The observed formation of *hP*3-Y instead of other yttrium allotropes is expected to be due to the applications of HT (i.e., k_BT equaling 0.172 eV at 2000 K, less than the calculated enthalpy difference at 20 GPa) during HP synthesis and stabilization of the metastable phase by rapid quenching down to room temperature.

The pressure dependence of the volume per yttrium atom (V_0/atom) for *hP*3-Y in comparison with that for previously known allotropes [18] is shown in Figs. 3 and S1 in the Supplemental Material [44]. As mentioned above, the structures of known yttrium allotropes, *hP*2, *hR*9, *hP*4, and *cF*4, differ only in the stacking of close-packed atomic layers, and their pressure-volume relations can be described by a single third-order Birch-Murnaghan (BM3) EoS with the following parameters: bulk modulus $K_0 = 29(1)$ GPa, V_0/atom = 34.5(4) Å^3, the pressure derivative of the bulk modulus $K_0' = 3.54(5)$ (Fig. S1 in the Supplemental Material [44]). Interestingly, although the allotrope *hP*3-Y has a different structure, the parameters of its BM3 EoS (based on the pressure-volume relation from DFT calculations for *hP*3-Y) are similar: $K_0 = 36(1)$ GPa, V_0/atom = 32.7(1) Å^3, $K_0' = 3.54(1)$. which is in good agreement with the BM3 fit of the data from Ref. [18] (Fig. S1 in the Supplemental Material [44]).

Previously, it has been shown that pressure induces $s \rightarrow d$ electron transfer that can play an important role in phase stabilization. Therefore, the phase transitions observed under pressure in many lanthanides and yttrium are common [19–21]. For a deeper understanding of the electronic properties of *hP*3-Y, we calculated the electronic band structure, the electronic density of states (eDOS), and Fermi surfaces of the two allotropes, *hP*2-Y (hcp) and *hP*3-Y, that exist at ambient conditions. Figures 4(a)–4(c) show the calculated total and partial eDOS at 1 bar. Both yttrium allotropes exhibit metallic properties, and the main contribution at the Fermi level for both phases comes from the *d* states, while *p* and *s* states make quite small contributions. A detailed inspection of the difference in the contribution of the *s* and *d* states to the total eDOS [insert in Fig. 4(c)] reveals that, during the transition

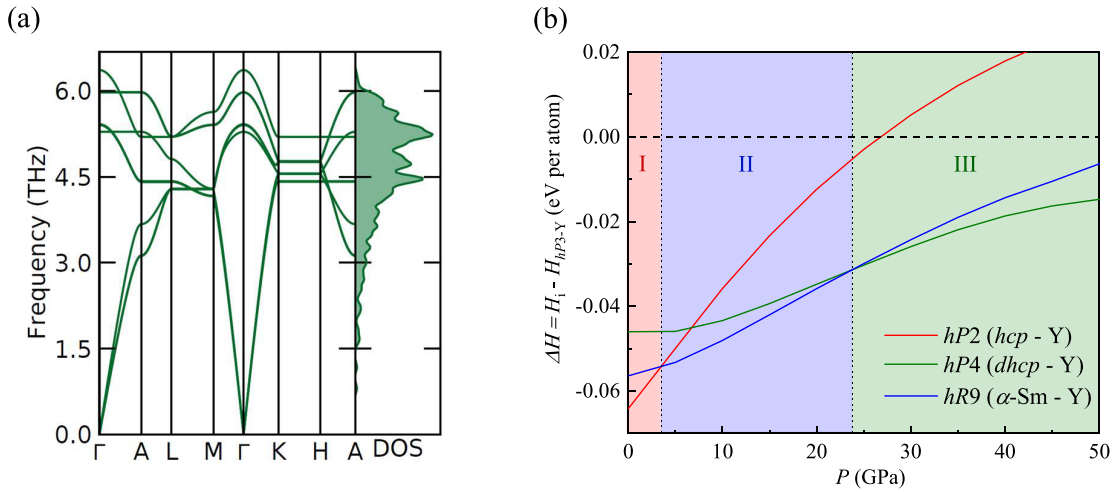

FIG. 2. Results of density functional theory (DFT) calculations. (a) Phonon dispersion curves for *hP*3-Y (*P*6/*mmm*) calculated at 1 bar along high-symmetry directions in the Brillouin zone and resulting phonon density of states. (b) Calculated enthalpy difference between known yttrium allotropes (hcp, α-Sm type, and dhcp) and *hP*3-Y: $\Delta H = H_i - H_{hP3-Y}$.

from *hP*2-Y to *hP*3-Y, the relative contribution of the *d* states to the density of states near the Fermi level increases from ~25% for *hP*2-Y to 75% for *hP*3-Y. Moreover, Fig. 4(a) shows a higher total eDOS at the Fermi level for *hP*3-Y than for *hP*2-Y. Usually, an increase in the eDOS at the Fermi energy strengthens the electron-phonon coupling, and as the range of phonon frequencies for *hP*3-Y [Fig. 2(a)] and *hP*2-Y [20] is very similar, one can assume a higher phonon-electron coupling constant for *hP*3-Y (i.e., potential superconductivity with enhanced T_C).

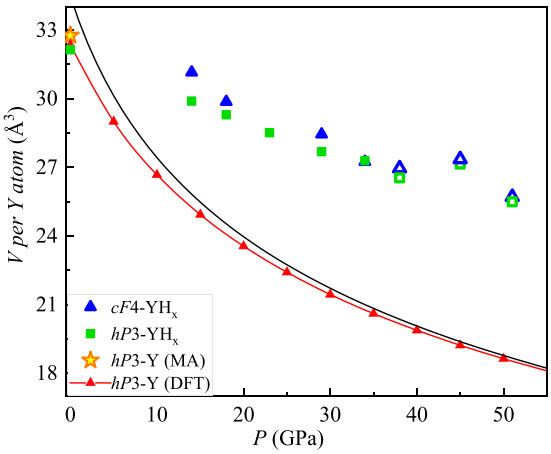

FIG. 3. Pressure dependence of the volume per yttrium atom for *hP*3-Y and yttrium hydrides, *hP*3-YH$_x$ and *cF*4-YH$_x$, determined in this paper. The literature data for previously known yttrium allotropes, fitted by a single Birch-Murnaghan (BM3) equation of state (EoS; black line), are given for comparison. All blue symbols represent experimental values for *cF*4-YH$_x$, green symbols for *hP*3-YH$_x$. Open and filled symbols represent data obtained at high-pressure–high-temperature (HP-HT) conditions and on decompression, respectively. The density functional theory (DFT)-calculated pressures for given volume for *hP*3-Y are shown by red triangles and solid line.

For a comparison of the properties of two yttrium allotropes, *hP*3-Y and *hP*2-Y, Fermi surfaces were calculated.

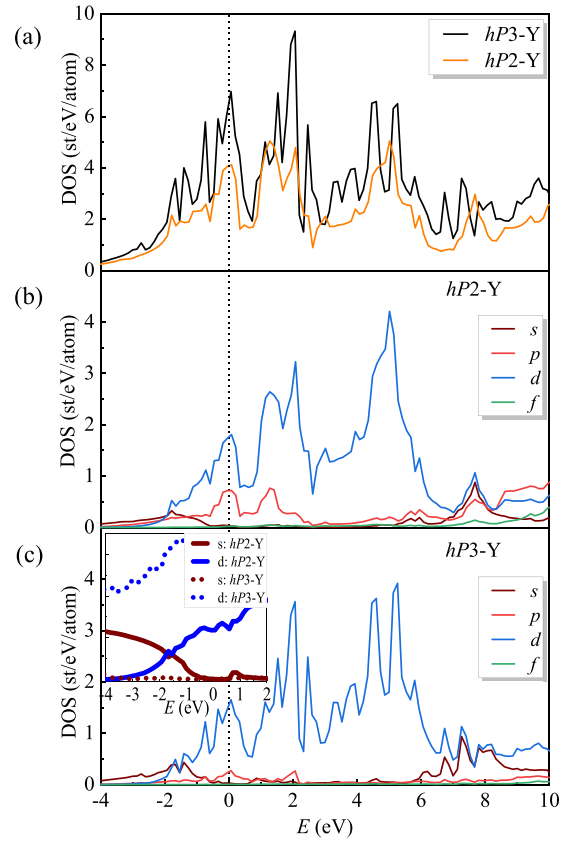

FIG. 4. Electronic density of states (eDOS) calculations at 1 bar. (a) Total eDOS for *hP*2-Y and *hP*3-Y. Partial eDOS for (b) *hP*2-Y and (c) *hP*3-Y. The inset in (c) shows relative contributions to the total eDOS of the *s* and *d* states for *hP*3-Y (dashed brown line = *s* states, dashed blue line = *d* states) and for *hP*2-Y (solid brown line = *s* states, solid blue line = *d* states). The vertical dashed line indicates the Fermi energy.

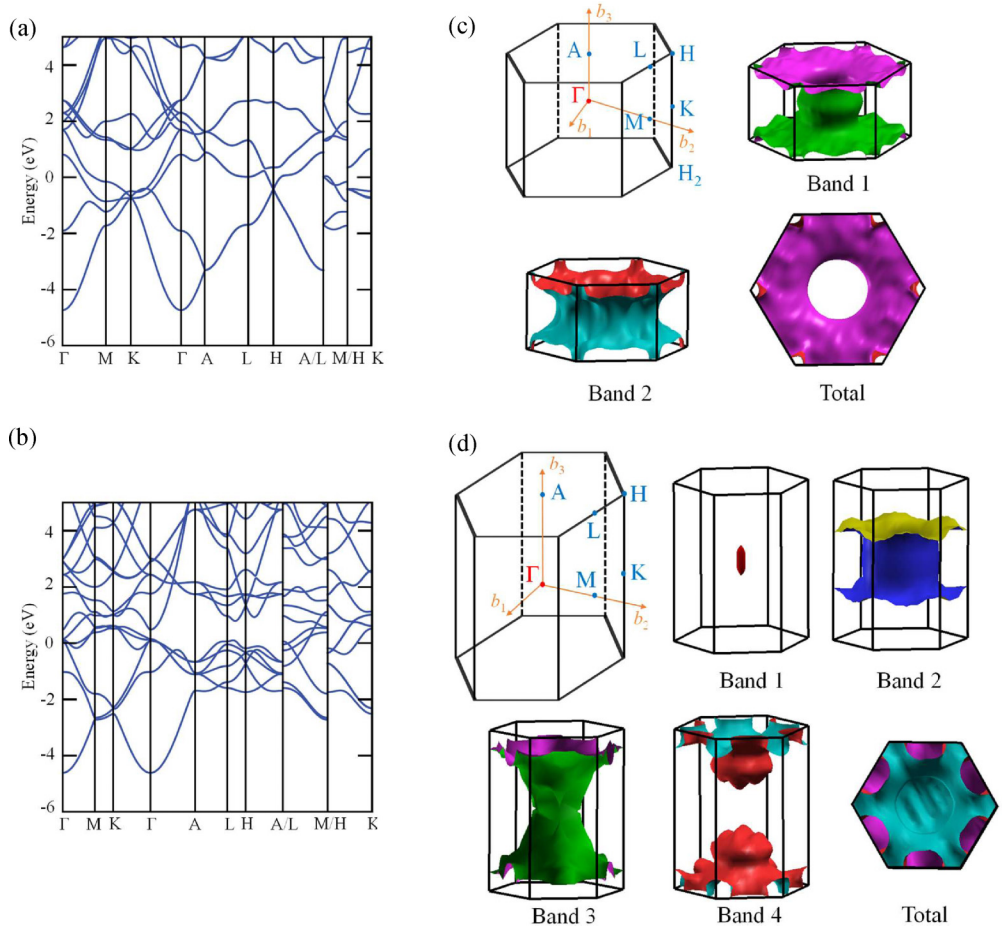

FIG. 5. Electronic band structure along high-symmetry directions in the hexagonal Brillouin zones of (a) *hP*2-Y and (b) *hP*3-Y at 1 bar. Brillouin zone and density functional theory (DFT)-calculated Fermi surfaces of (c) *hP*2-Y and (d) *hP*3-Y at 1 bar.

Figure 5 shows calculated band structures along high-symmetry directions in the hexagonal Brillouin zones *hP*3-Y and *hP*2-Y at ambient pressure. In the case of *hP*2-Y, two bands cross the Fermi energy; for *hP*3-Y, multiple electronic bands. As a result, the yttrium allotrope has a more complicated Fermi surface with a higher amount of contributing Fermi subsurfaces than *hP*2-Y (Fig. 5). The geometrical characteristics of the Fermi surfaces, such as the shape, curvature, and cross-sectional area, are related to the physical properties of metals such as electronic transport, specific heat, magnetic susceptibility, and optical absorption [48,49].

In *hP*2-Y, both bands cross the Fermi level, giving rise to two open distorted cylindricallike tubes with different radii along the Γ-*A* direction in the Brillouin zone, together forming a honeycomblike structure with hexagonal symmetry [Fig. 5(c)]. By contrast, the Fermi surface of *hP*3-Y consists not only of open surfaces with irregular shapes but also contains a closed surface and Fermi pockets that are restricted within the first Brillouin zone [Band 1 around the Γ point and Band 4 around the *A* point at the Brillouin zone boundary in Fig. 5(d)]. For some systems, it has been shown that the presence of coexisting Fermi pockets and Fermi surface nesting can indicate a strong electron-phonon coupling and hence potentially interesting electronic properties including superconductivity [50–52]. For titanium, which has a similar $hP2 \rightarrow hP3$ transition, it was shown that the holelike or electronlike Fermi pockets and nesting features that appear at the Fermi surface during pressure-induced phase transitions $\alpha(P6_3/mmc) \rightarrow \omega(P6/mmm) \rightarrow \gamma(Cmcm) \rightarrow \delta(Cmcm)$ [53] (Fig. S2 in the Supplemental Material [44]) substantially enhance the electron-phonon coupling and result in an increase of T_C (from 0.5 K at 1 bar for α-Ti to 2.3 K at 40.9 GPa for ω-Ti, with the maximum $T_C = 23.6$ K at 145 GPa for δ-Ti) [53,54]. Yttrium metal at ambient pressure has T_C of 6 mK [55]; however, it drastically increases with pressure (1.3 K at 11 GPa [56] and 19.5 K at 115 GPa [57]). The value of dT_C/dP for pressures < 50 GPa for yttrium is higher than for Ti [53]; therefore, one can expect enhanced superconductivity for *hP*3-Y.

The synthesis of a yttrium allotrope at HP-HT conditions indicates that yet unknown hydrides may exist at the same conditions. To check this, we studied chemical reactions between yttrium and three different hydrogen-rich precursors—hydrogen gas, paraffin oil, and ammonia borane—in the pressure range between 38 and 51 GPa upon heating up to ~3400 K (Tables S1 and S3 in the Supplemental Material [44]). Regardless of the hydrogen source, two kinds of yttrium hydrides YH_x were synthesized: Y frameworks were either in the cubic (*Fm*-3*m*) or hexagonal (*P*6/*mmm*) structures, hereafter named *cF*4-YH_x and *hP*3-YH_x phases,

respectively. For example, at the highest pressure reached in this paper (51 GPa), a reaction between Y and paraffin oil led to the formation of both $hP3$-YH_x [$a = 5.299(1)$ Å, $c = 3.145(7)$ Å, and $V = 76.48(17)$ Å^3] and $cF4$-YH_x [$a = 4.685(1)$ Å and $V = 102.81(5)$ Å^3] with yttrium atoms on the nodes of the fcc lattice (Table S3 in the Supplemental Material [44]). Additionally, in the experiment with paraffin oil as a hydrogen precursor, we obtained two previously unknown yttrium carbides (Table S1 in the Supplemental Material [44]), which we have already described in Ref. [12].

The positions of yttrium atoms in hydrides were determined from SCXRD. The positions of the light hydrogen atoms could not be found from XRD data, and therefore, only the hydrogen content was estimated based on the difference in volume per yttrium atom between hydrides YH_x and yttrium metal at the same pressure [18], using a previously established pressure dependence of the volume per atomic H [58]. The evaluated stoichiometries for yttrium hydrides at each pressure point are given in Table S3 in the Supplemental Material [44]. Due to the systematic theoretical errors of the atomic hydrogen pressure-volume dependence model [58], the uncertainties of the hydrogen content in yttrium hydrides are difficult to estimate and therefore are not given.

During decompression (Table S3 in the Supplemental Material [44], Fig. 3) both hexagonal and cubic hydrides, $hP3$-YH_x and $cF4$-YH_x, gradually lost hydrogen (from $x = 2.9$ at 51 GPa to $x = 1.4$ at 14 GPa). At ambient conditions, hydrogen was fully released, and only $hP3$-Y was recovered. The volume per Y atom of the $hP3$-Y decompressed in DAC2 [$V = 32.32(2)$ Å^3] is consistent with that of the $hP3$-Y sample obtained from MA experiments [$V = 32.76(4)$ Å^3] and of $hP2$-Y [$V = 33.01(6)$ Å^3] [18]. Thus, the YH_x phases (both cubic and hexagonal) behave like metal-hydrogen solid solutions. The pressure-volume relation observed for hydrides synthesized from paraffin oil and ammonia borane as a hydrogen reservoir (DAC1 and DAC2) are similar (Fig. 3), but the cubic hydride contains a little bit more hydrogen than the hexagonal one at the same pressure (Fig. 3 and Table S3 in the Supplemental Material [44]).

The discovery of a Y allotrope, $hP3$-Y, and its derivative YH_x hydrides significantly extends the Y and Y-H phase diagrams at moderate pressures (up to 51 GPa). Since RE metals and their known hydrides usually behave similarly at HP-HT conditions, it is important to examine if other RE metals also form $hP3$-RE hydrides. We tested this on Nd and Gd metals that we laser heated to ∼3000 K in paraffin oil at 40 and 45 GPa, leading to the synthesis of $hP3$-NdH_4 and $hP3$-$GdH_{3.5}$ (see information for DAC4 and DAC5 in Table S1 in the Supplemental Material [44]). In addition, at 40 GPa, a cubic $cF4$-$NdH_{4.1}$ (with fcc metal lattice) was observed with the same (within uncertainty) volume per Nd atom as in $hP3$-NdH_4, i.e., with the same hydrogen content. Upon decompression of DAC4, NdH_x hydrides (both cubic and hexagonal) lost hydrogen (at 24 GPa, $x = 3$; at 4 GPa, $x = 0.7$; Table S4 in the Supplemental Material [44]), showing a behavior like that of yttrium hydrides discussed above. This suggests that $hP3$-$(RE)H_x$ hydrides may be common for RE metals, and their existence and properties should be considered in a broad context of studies on different aspects of the HP behavior of RE hydrides, particularly with respect to superconductivity.

V. CONCLUSIONS

To summarize, the HP-HT approach allowed us to synthesize a yttrium allotrope, hexagonal $hP3$-Y, recoverable to ambient conditions. DFT-based phonons calculations confirm its dynamic stability at 1 bar. The enthalpy calculations showed that $hP3$-Y is metastable up to 50 GPa but may be synthesized at HP-HT conditions and stabilized by rapid quenching. With a detailed analysis of the electronic structure of the yttrium allotrope from DFT calculations, the stabilization of $hP3$-Y can be rationalized in terms of electronic $s \rightarrow d$ transfer, a mechanism common for lanthanides. We have further shown that, at HP-HT conditions, $hP3$-Y can dissolve a significant amount of hydrogen (up to 3 hydrogen atoms per 1 yttrium atom) through a direct reaction of yttrium with different hydrogen-rich precursors. Decompression experiments revealed the release of hydrogen with decreasing pressure, leading to the formation of hydrides with variable hydrogen content. Isostructural $hP3$-$(RE)H_x$ hydrides (RE = Nd and Gd) were obtained, which suggests that the structure type may be common for RE elements. Thus, our results enrich the Y phase diagram and suggest that it is important to further study the structural phase transitions in other RE metals and their hydrides.

ACKNOWLEDGMENTS

The authors acknowledge the DESY, PETRA III for the provision of beamtime at the P02.2 and the ESRF for the provision of beamtime at the ID15b beamline. D.L. thanks the UKRI Future Leaders Fellowship (No. MR/V025724/1) for financial support. N.D. and L.D. thank the Federal Ministry of Education and Research, Germany (Grant No. 05K19WC1) and the Deutsche Forschungsgemeinschaft (DFG Projects No. DU 954–11/1, No. DU 393–9/2, and No. DU 393–13/1) for financial support. N.D. also thanks the Swedish Government Strategic Research Area in Materials Science on Functional Materials at Linköping University (Faculty Grant SFO-Mat-LiU No. 2009 00971). G.S.N. acknowledges financial support by DFG through Project No. STE1105/13-2 in the Research Unit FOR2440. For open access, the author has applied a Creative Commons Attribution (CC BY) license to any author accepted manuscript version arising from this submission.

[1] J. A. Flores-Livas, L. Boeri, A. Sanna, G. Profeta, R. Arita, and M. Eremets, Phys. Rep. **856**, 1 (2020).

[2] A. P. Drozdov, P. P. Kong, V. S. Minkov, S. P. Besedin, M. A. Kuzovnikov, S. Mozaffari, L. Balicas, F. F. Balakirev, D. E. Graf, V. B. Prakapenka *et al.*, Nature (London) **569**, 528 (2019).

[3] M. Somayazulu, M. Ahart, A. K. Mishra, Z. M. Geballe, M. Baldini, Y. Meng, V. V. Struzhkin, and R. J. Hemley, Phys. Rev. Lett. **122**, 027001 (2019).

[4] N. P. Salke, M. M. Davari Esfahani, Y. Zhang, I. A. Kruglov, J. Zhou, Y. Wang, E. Greenberg, V. B. Prakapenka, J. Liu, A. R. Oganov *et al.*, Nat. Commun. **10**, 4453 (2019).

[5] I. A. Kruglov, A. G. Kvashnin, A. F. Goncharov, A. R. Oganov, S. S. Lobanov, N. Holtgrewe, S. Jiang, V. B. Prakapenka, E. Greenberg, and A. V. Yanilkin, Sci. Adv. **4**, eaat9776 (2018).

[6] D. V. Semenok, A. G. Kvashnin, A. G. Ivanova, V. Svitlyk, V. Y. Fominski, A. V. Sadakov, O. A. Sobolevskiy, V. M. Pudalov, I. A. Troyan, and A. R. Oganov, Mater. Today **33**, 36 (2020).

[7] P. Kong, V. S. Minkov, M. A. Kuzovnikov, A. P. Drozdov, S. P. Besedin, S. Mozaffari, L. Balicas, F. F. Balakirev, V. B. Prakapenka, S. Chariton *et al.*, Nat. Commun. **12**, 5075 (2021).

[8] I. A. Troyan, D. V. Semenok, A. G. Kvashnin, A. V. Sadakov, O. A. Sobolevskiy, V. M. Pudalov, A. G. Ivanova, V. B. Prakapenka, E. Greenberg, A. G. Gavriliuk *et al.*, Adv. Mater. **33**, 2006832 (2021).

[9] E. Snider, N. Dasenbrock-Gammon, R. McBride, X. Wang, N. Meyers, K. V. Lawler, E. Zurek, A. Salamat, and R. P. Dias, Phys. Rev. Lett. **126**, 117003 (2021).

[10] J. E. Hirsch and F. Marsiglio, Matter Radiat. Extrem. **7**, 058401 (2022).

[11] J. E. Hirsch and F. Marsiglio, Phys. Rev. B **103**, 134505 (2021).

[12] D. Laniel, B. Winkler, E. Bykova, T. Fedotenko, S. Chariton, V. Milman, M. Bykov, V. Prakapenka, L. Dubrovinsky, and N. Dubrovinskaia, Phys. Rev. B **102**, 134109 (2020).

[13] T. Meier, F. Trybel, S. Khandarkhaeva, G. Steinle-Neumann, S. Chariton, T. Fedotenko, S. Petitgirard, M. Hanfland, K. Glazyrin, N. Dubrovinskaia *et al.*, Phys. Rev. X **9**, 031008 (2019).

[14] T. Meier, F. Trybel, G. Criniti, D. Laniel, S. Khandarkhaeva, E. Koemets, T. Fedotenko, K. Glazyrin, M. Hanfland, M. Bykov *et al.*, Phys. Rev. B **102**, 165109 (2020).

[15] T. Meier, A. Aslandukova, F. Trybel, D. Laniel, T. Ishii, S. Khandarkhaeva, N. Dubrovinskaia, and L. Dubrovinsky, Matter Radiat. Extrem. **6**, 068402 (2021).

[16] A. Aslandukova, A. Aslandukov, L. Yuan, D. Laniel, S. Khandarkhaeva, T. Fedotenko, G. Steinle-Neumann, K. Glazyrin, N. Dubrovinskaia, and L. Dubrovinsky, Phys. Rev. Lett. **127**, 135501 (2021).

[17] A. F. Goncharov, E. Bykova, M. Bykov, X. Zhang, Y. Wang, S. Chariton, V. B. Prakapenka, and J. S. Smith, J. Appl. Phys. **131**, 025902 (2022).

[18] E. J. Pace, S. E. Finnegan, C. V. Storm, M. Stevenson, M. I. McMahon, S. G. MacLeod, E. Plekhanov, N. Bonini, and C. Weber, Phys. Rev. B **102**, 094104 (2020).

[19] J. C. Duthie and D. G. Pettifor, Phys. Rev. Lett. **38**, 564 (1977).

[20] P. P. Singh, Phys. Rev. B **75**, 125101 (2007).

[21] H. Olijnyk, J. Phys. Condens. Matter **17**, 43 (2005).

[22] R. J. Wijngaarden, J. N. Huiberts, D. Nagengast, J. H. Rector, R. Griessen, M. Hanfland, and F. Zontone, J. Alloys Compd. **308**, 44 (2000).

[23] A. Machida, A. Ohmura, T. Watanuki, K. Aoki, and K. Takemura, Phys. Rev. B **76**, 052101 (2007).

[24] A. Machida, A. Ohmura, T. Watanuki, T. Ikeda, K. Aoki, S. Nakano, and K. Takemura, Solid State Commun. **138**, 436 (2006).

[25] D. J. Frost, B. T. Poe, R. G. Trønnes, C. Liebske, A. Duba, and D. C. Rubie, Phys. Earth Planet. Inter. **143**, 507 (2004).

[26] I. Kantor, V. Prakapenka, A. Kantor, P. Dera, A. Kurnosov, S. Sinogeikin, N. Dubrovinskaia, and L. Dubrovinsky, Rev. Sci. Instrum. **83**, 125102 (2012).

[27] Rigaku Oxford Diffraction, CRYSALISPRO Software system (2015).

[28] C. S. Zha, W. A. Bassett, and S. H. Shim, Rev. Sci. Instrum. **75**, 2409 (2004).

[29] S. Anzellini, A. Dewaele, F. Occelli, P. Loubeyre, and M. Mezouar, J. Appl. Phys. **115**, 043511 (2014).

[30] Y. Akahama and H. Kawamura, J. Appl. Phys. **100**, 043516 (2006).

[31] T. Fedotenko, L. Dubrovinsky, G. Aprilis, E. Koemets, A. Snigirev, I. Snigireva, A. Barannikov, P. Ershov, F. Cova, M. Hanfland *et al.*, Rev. Sci. Instrum. **90**, 104501 (2019).

[32] CRYSALISPRO Data Collection and Processing Software for Agilent X-ray Diffractometers.

[33] A. Aslandukov, M. Aslandukov, N. Dubrovinskaia, and L. Dubrovinsky, J. Appl. Cryst. **55**, 1383 (2022).

[34] O. V. Dolomanov, L. J. Bourhis, R. J. Gildea, J. A. K. Howard, and H. Puschmann, J. Appl. Cryst. **42**, 339 (2009).

[35] V. Petrícek, M. Dušek, and L. Palatinus, Z. Kristallogr. Cryst. Mater. **229**, 345 (2014).

[36] G. M. Sheldrick, Acta Cryst. C **71**, 3 (2015).

[37] K. Momma and F. Izumi, J. Appl. Cryst. **44**, 1272 (2011).

[38] J. Gonzalez-Platas, M. Alvaro, F. Nestola, and R. Angel, J. Appl. Cryst. **49**, 1377 (2016).

[39] J. P. Perdew, K. Burke, and M. Ernzerhof, Phys. Rev. Lett. **77**, 3865 (1996).

[40] G. Kresse and D. Joubert, Phys. Rev. B **59**, 1758 (1999).

[41] G. Kresse and J. Furthmüller, Phys. Rev. B **54**, 11169 (1996).

[42] A. Togo and I. Tanaka, Scr. Mater. **108**, 1 (2015).

[43] A. Kokalj, J. Mol. Graph. Model. **17**, 176 (1999).

[44] See Supplemental Material at http://link.aps.org/supplemental/10.1103/PhysRevB.107.014103 for the full description of the sample preparation, the full crystallographic details on the structures solved by SCXRD, as well as complementary figures.

[45] V. Babizhetskyy, B. Kotur, V. Levytskyy, and H. Michor, in *Handbook on the Physics and Chemistry of Rare Earths*, edited by J.-C. G. Bünzli and V. K. Pecharsky (Elsevier, Amsterdam, 2017), Vol. 52, pp. 1–263.

[46] E. S. Chebotareva and S. G. Nuzhdina, Phys. Metals Metallogr. **36**, 200 (1973).

[47] M. Sabeena, S. Murugesan, P. Anees, E. Mohandas, and M. Vijayalakshmi, J. Alloys Compd. **705**, 769 (2017).

[48] W. A. Harrison and R. W. Schmitt, Phys. Today **14**, 20 (1961).

[49] B. Zimmermann, P. Mavropoulos, N. H. Long, C. R. Gerhorst, S. Blügel, and Y. Mokrousov, Phys. Rev. B **93**, 144403 (2016).

[50] C. M. Hao, Y. Li, H. M. Huang, Y. Li, and Y. L. Li, Inorg. Chem. **59**, 484 (2020).

[51] S. Lebègue, Phys. Rev. B **75**, 035110 (2007).

[52] D. Kasinathan, J. Kuneš, A. Lazicki, H. Rosner, C. S. Yoo, R. T. Scalettar, and W. E. Pickett, Phys. Rev. Lett. **96**, 047004 (2006).

[53] X. Liu, P. Jiang, Y. Wang, M. Li, N. Li, Q. Zhang, Y. Wang, Y.-L. Li, and W. Yang, Phys. Rev. B **105**, 224511 (2022).

[54] I. O. Bashkin, V. G. Tissen, M. V. Nefedova, and E. G. Ponyatovsky, Phys. C Supercond. Appl. **453**, 12 (2007).

[55] C. Probst and J. Wittig, in *Handbook on the Physics and Chemistry of Rare Earths* (Elsevier, Amsterdam, 1978), Vol. 1, pp. 749–795.

[56] J. Wittig, Phys. Rev. Lett. **24**, 812 (1970).

[57] J. J. Hamlin, V. G. Tissen, and J. S. Schilling, Phys. C Supercond. Appl. **451**, 82 (2007).

[58] B. Guigue, A. Marizy, and P. Loubeyre, Phys. Rev. B **102**, 014107 (2020).